RSC Advances

PAPER

View Article Online
View Journal | View Issue

Cite this: *RSC Adv.*, 2020, **10**, 18687

Room temperature ferromagnetism in D–D neutron irradiated rutile TiO_2 single crystals

Huan Liu,[a] Gongping Li, *[a] Dejun E,[a] Nannan Xu,[b] Qiaolu Lin,[a] Xudong Gao,[a] Changlin Lan,[a] Jingsheng Chen,[c] Canglong Wang,[b] Xuwen Zhan[a] and Kai Zhang[d]

Received 10th March 2020
Accepted 20th April 2020

DOI: 10.1039/d0ra02220a

rsc.li/rsc-advances

Room temperature ferromagnetism (RTFM) was observed in unirradiated rutile TiO_2 single crystals prepared by the floating zone method due to oxygen vacancy (V_O) defects. D–D neutrons mainly collide elastically with TiO_2, producing V_O, titanium vacancies (V_{Ti}) and other point defects; the density and kind of defect is related to the neutron irradiation fluence. D–D neutron irradiation is used to regulate the concentration and type of defect, avoiding impurity elements. As the irradiation fluence increases, the saturation magnetization (M_s) first increases, then decreases and then increases. To verify the origin of RTFM, the CASTEP module was used to calculate the magnetic and structural properties of point defects in TiO_2. V_O induces a 2.39 μ_B magnetic moment, Ti^{3+} and F^+ induce 1.28 μ_B and 1.70 μ_B magnetic moments, respectively, while V_{Ti} induces a magnetic moment of ~4 μ_B. Combining experimental and theoretical results, increases in V_O concentration lead to M_s increases; more V_O combine with electrons to form F^+, inducing a smaller magnetic moment. V_O and V_{Ti} play a key role and M_s changes accordingly with larger fluence. V_O, F^+ and V_{Ti} are the most likely origins of RTFM.

1 Introduction

TiO_2 is a versatile functional material that has important applications[1–3] in the fabrication of spintronics, optical coatings and solar cells. TiO_2 doped with different ions has been synthesized[4–6] to modify its ferromagnetic and optical properties. TiO_2 also has outstanding magnetic properties, showing RTFM in both ion-doped and undoped states. However, there is no consensus on the origin of magnetism of TiO_2, and some experimental results contradict each other. Kaspar *et al.*[7] pointed out that extended structural defects appear to be necessary to promote ferromagnetic ordering in Cr:TiO_2. Saadaoui *et al.*[8] found that the ferromagnetism is intrinsic and controlled by oxygen vacancies. Zheng *et al.*[9] reported that oxygen defects can be the dominating factor for increasing the saturation moment of Cu-doped TiO_2 film. Zhou *et al.*[10] found that ferromagnetism was related to a lower level of V_O defects. Parras *et al.*[11] pointed out that the magnetic moment is indeed due to the Ti^{3+} ions induced by reduction. Wang *et al.*[12] reported that V_{Ti} could be the origin of RTFM.

Defects play an important role in the structural, magnetic and optical properties of semiconductor materials; in particular, the intrinsic defects of TiO_2 have the potential to induce spintronic properties at room temperature. Magnetic semiconductors with high Curie temperatures are expected to be used in spintronic materials with great potential applications because they can utilize both charge and spin degrees of freedom in a single component. Venhatesan and Coey *et al.*[13] reported that HfO_2 films have high-temperature ferromagnetism and first proposed the concept of d^0 magnetism. They avoided the interference of the second phase of magnetic elements in dilute magnetic semiconductors (DMS) and only studied the effect of intrinsic defects. Since then, many research groups have studied defects causing RTFM in TiO_2-based DMS materials.

In our previous work, the magnetic properties of Cu-doped TiO_2 were investigated[14,15] by theoretical and experimental studies. RTFM may be induced by V_O or Cu^{2+}–V_O; the effects of intrinsic defects and Cu-doping are ambiguous. The effects of γ-ray and D–D neutron irradiation[16,17] on the RTFM of TiO_2 single crystals were initially explored. RTFM was observed, and V_O was the main origin of room temperature ferromagnetism. D–D neutrons mainly scatter with TiO_2 single crystals; they have the right energy to cause vacancy defects, but not to produce a nuclear reaction at a higher energy or capture neutrons at a lower energy. Furthermore, because D–D neutron fluence could regulate the concentration and kind of defect, it is beneficial to explore the effect of intrinsic defects on RTFM properties. The effects of different defect concentrations and types on ferromagnetism can be obtained by adjusting the neutron fluence. Using D–D neutron irradiation has significant

[a]School of Nuclear Science and Technology, Lanzhou University, Lanzhou, Gansu 730000, China. E-mail: ligp@lzu.edu.cn
[b]Institute of Modern Physics, Chinese Academy of Sciences, Lanzhou, Gansu 730000, China
[c]Department of Materials Science and Engineering, National University of Singapore, Singapore 117608, Singapore
[d]China Institute of Atomic Energy, Beijing 102413, China

advantages over doping with other magnetic elements to clarify the origin of RTFM.

In this study, to illustrate the effect of intrinsic defects on magnetic and structural properties and optical band gap, D–D neutron irradiation was carried out to verify the effect of intrinsic defects in rutile TiO_2 single crystals. In addition, we use the CASTEP module based on a density functional theory (DFT) method to calculate the magnetic properties of intrinsic vacancy defects. This lays a foundation for the application of TiO_2 in photocatalysis and spintronics.

2 Materials and methods

Pure TiO_2 single crystals from MaTeck prepared by the floating zone method with one side polished were cut to 5 × 10 × 0.5 mm^3. D–D neutron irradiation with fluences of 0 n cm^{-2}, 2 × 10^9 n cm^{-2}, 5 × 10^9 n cm^{-2}, 1 × 10^{10} n cm^{-2}, and 2.5 × 10^{10} n cm^{-2} was used.

X-ray diffraction (XRD, D/Max-2400) with Cu K_α radiation ($\lambda = 0.15406$ nm) was used to characterize the structure of TiO_2. The working voltage is 40 kV, the working current is 60 mA, the step length is 0.02°, the scanning speed is 20° min^{-1}, and the scanning range is 20–80°. The excitation wavelength of the Raman spectrum is 532 nm, the laser power of the backscattering mode is 10 mW, and the spot size is 2 μm. The Raman displacement range is 100–1000 cm^{-1} and the integral time is 10 s. Three points were selected from each sample for testing. A superconducting quantum interferometer (SQUID) was used to measure the M–H curves under an external magnetic field parallel to the surface of the sample. X-ray photoelectron spectroscopy (XPS) was conducted using a PHI-5702 multifunctional electronic spectrometer. A conductive adhesive was used to stick the sample to the sample rack, with the polished surface facing out. The wide spectra (0–1000 eV), Ti (450–468 eV) and O (525–537 eV), and C (274–296 eV) fine spectra were tested, respectively. The photon energy of the X-ray source with Al as the anode material is 1486.6 eV. The photoluminescence (PL) source is a xenon lamp with an excitation source wavelength of 415 nm and a spectral range of 450–750 nm. Electron spin resonance (ESR) spectra were tested on a Bruker EMX plus at 2 K at the Steady High Magnetic Field Facilities, High Magnetic Field Laboratory, CAS. The samples were cut to 2 mm × 2 mm for testing. The magnetic field range is 2900–3900 G and the microwave frequency is 9.4 GHz. The ultraviolet visible (UV-vis) spectra were obtained in reflection mode with the measurement range of 300–700 nm.

3 Results and discussion

Fig. 1 represents the XRD patterns after neutron irradiation. There are TiO_2 (002) and Cu K_α peaks in the spectra. The full width at half maximum (FWHM) of the (002) peak is very small, indicating that the single crystals have high crystallinity. The (002) peak shows a small shift toward a small angle, which means that the lattice expands a little due to the repulsion force between the oxygen vacancies. Fig. 1(b) shows two small peaks

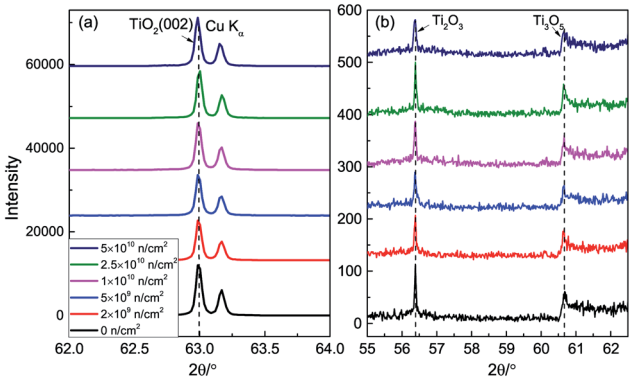

Fig. 1 XRD patterns; (a) (002) peak and (b) drawing of partial enlargement of TiO_2 before and after neutron irradiation.

at 56.4° and 60.7°, corresponding to Ti_2O_3 and Ti_3O_5, which indicates that TiO_2 is non-stoichiometric.

The space group[18] of rutile TiO_2 is $D_{4h}{}^{14}$, and the Raman-active vibrational energy levels are B_{1g} (143 cm^{-1}), E_g (447 cm^{-1}), A_{1g} (611 cm^{-1}), and B_{2g} (828 cm^{-1}). The scattering intensity is proportional to the number of corresponding molecules and is related to the smoothness of the surface and diffuse reflection. The Raman spectra of the samples before and after irradiation are presented in Fig. 2. There is an asymmetrical broad peak at 235 cm^{-1}, corresponding to the second-order scattering of phonons or internal disorder. The damage can be described by the FWHM of the A_{1g} peaks; as the irradiation fluence increases, the A_{1g} peak still maintains a good FWHM. No peak shift or new vibration level was observed, which indicates that no obvious lattice damage was caused by neutron irradiation.

Fig. 3 illustrates the M–H curves before and after D–D neutron irradiation. All the samples exhibit RTFM, including the unirradiated sample, which agrees with the experimental results[19] and our preliminary work.[17] Oxygen deficiencies are inevitably introduced in the preparation by the floating zone method;[20,21] V_O would induce a magnetic moment. Santara *et al.*[19] reported that V_O induced strong ferromagnetism at and

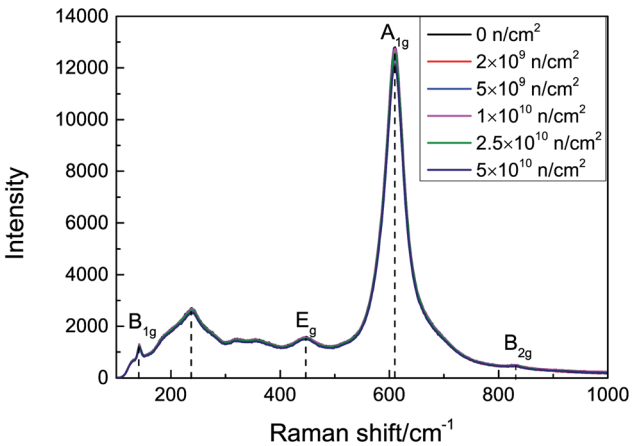

Fig. 2 Raman spectra of TiO_2 before and after neutron irradiation.

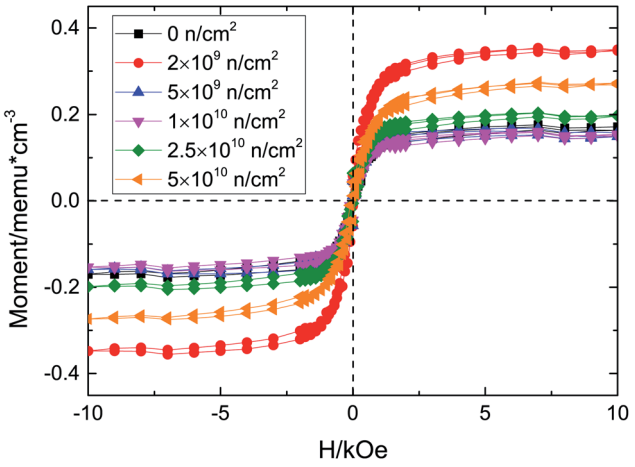

Fig. 3 M–H curves of TiO_2 before and after neutron irradiation.

above room temperature in undoped TiO_2 nanoporous nanoribbons. Furthermore, Kim *et al.*[22] pointed out that oxygen vacancy defects play an important role in the ferromagnetism of undoped rutile TiO_2. Moreover, our previous work,[17] using γ-ray irradiated TiO_2, also found that the origin of RTFM of unirradiated TiO_2 single crystals was V_O; thus the RTFM of unirradiated TiO_2 is due to V_O. D–D neutron irradiation has advantages in regulating the concentrations and kinds of defect; because of its energy it only collides with atoms in elastic scattering and the nuclear reaction cross section is 0, so no nuclear reaction occurs. Therefore, D–D neutron irradiation has been used to regulate defect concentration and type to study changes of RTFM.

The maximum saturation magnetization (M_s) is in the 2×10^9 n cm^{-2} sample, while the M_s of the 5×10^9 n cm^{-2} and 1×10^{10} n cm^{-2} samples are almost equal to that of the unirradiated sample. Then, the M_s increased with the irradiation fluence, which means that there is an optimal value for V_O defect concentration. D–D neutron irradiation mainly causes point vacancy defects. Considering the XRD and Raman results and the physical process of D–D neutron irradiation of TiO_2, the ferromagnetism may due to vacancy defects, such as V_O, V_{Ti}, and so on. In our previous work, we found that V_O could induce ~2 μ_B magnetic moment, while V_{Ti} could introduce ~4 μ_B magnetic moment, which we will verify below. After D–D neutron irradiation, V_O and V_{Ti} are induced due to the elastic collisions between neutrons and Ti and O atoms; these defects increase M_s. For the 5×10^9 n cm^{-2} and 1×10^{10} n cm^{-2} samples, M_s decreases on account of the compound defects that V_O make up with other defects,[10] *e.g.*, F^+, V_O–Ti^{3+}; these defects provide a smaller magnetic moment, so the total magnetic moment of the system is decreased. We preliminarily studied the Doppler broadening and positron annihilation spectroscopy[16,23,24] of Cu-doped and D–D neutron irradiated TiO_2, and V_{Ti} was found after spectral analysis. V_{Ti} would certainly be generated after D–D neutron irradiation of TiO_2 single crystals. Below, we will further investigate the increase due to the V_{Ti} and V_O defects produced when the fluence increased for the 2.5×10^{10} n cm^{-2} and 5×10^{10} n cm^{-2} samples.

The valence of Ti after irradiation was characterized by XPS spectra.[25–27] Only Ti, O and C could be detected. Using C 1 s (284.6 eV) for charge correction, the Ti 2p core electron spectra of the unirradiated and 2×10^9 n cm^{-2} samples are shown in Fig. 4. The peak separation fitting of the Ti 2p spectra was performed by the Gauss–Lorentz function. The Ti^{4+} $2p_{3/2}$ and $2p_{1/2}$ binding energies were 458.5 eV and 464.2 eV, respectively, and the energy level spacing[28,29] was 5.7 eV for Ti^{4+} and 5.2 eV for Ti^{3+}. After peak-differentiation and imitation, the unirradiated sample still showed +4 valence. Ti^{3+} was produced in irradiated TiO_2, proving that V_O was indirectly generated after irradiation. Ti^{3+} contributes a paramagnetic signal,[30] and the Ti^{3+} peak area shows no obvious change with the increased irradiation dose, which is inconsistent with the change of M_s.

To investigate the defect type after neutron irradiation, PL spectra are displayed in Fig. 5(a). After peak separation, the three main peaks are centered at 473 nm (2.62 eV), 600 nm (2.07 eV) and 820 nm (1.51 eV), as shown in Fig. 5(b). As the PL spectra are similar, we choose the 2×10^9 n cm^{-2} sample for detailed analysis. In TiO_2, the electron trap state caused by V_O is about 0.5–1 eV below the bottom of the conduction band.[31] Therefore, the band peak at 473 nm is assigned to V_O and the deep level emission[32,33] of V_O, which is consistent with the first principles calculation below. The 600 nm luminescence peak is attributed to the consequence of polarization of the lattice ions surrounding the vacancy.[34] The peak at 818 nm might be

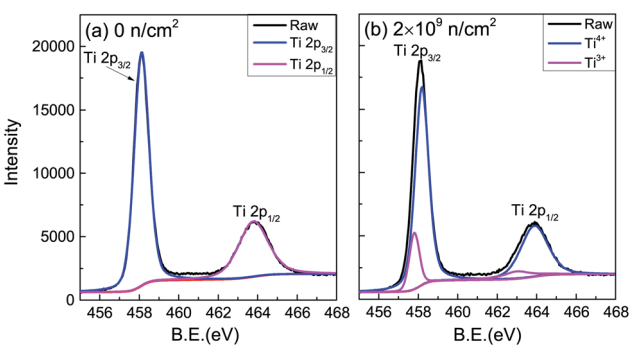

Fig. 4 XPS spectra of (a) raw and (b) 2×10^9 n cm^{-2} TiO_2 samples.

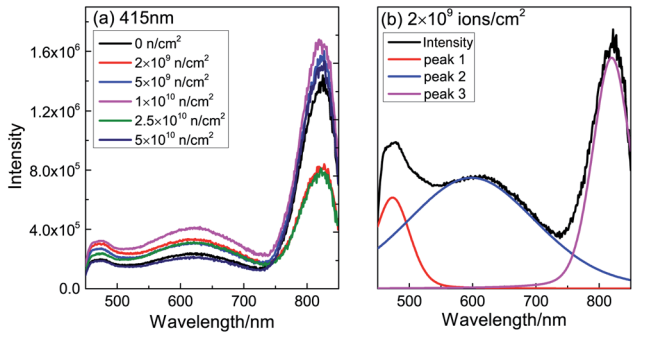

Fig. 5 (a) Raw PL spectra of TiO_2 before and after neutron irradiation and (b) normalized PL spectra for 2×10^9 n cm^{-2}.

Table 1 Peak area of PL spectra after peak fitting

Sample (n cm^{-2})	473 nm	600 nm	820 nm
0	0.0777	0.3424	0.5798
2×10^9	0.1195	0.5308	0.3496
5×10^9	0.0889	0.3729	0.5382
1×10^{10}	0.0871	0.4241	0.4888
2.5×10^{10}	0.0970	0.5195	0.3835
5×10^{10}	0.0751	0.2944	0.6305

a consequence of Ti^{3+} or F^+ defects. Table 1 shows the area of the peaks after normalization. The area of the 473 nm peak is found to vary according to the change of M_S; this is direct evidence that V_O causes RTFM. With the increase of neutron injection, V_O gradually forms an extinction center; more and more V_O combine with electrons to form F^+.[35] F^+ induce a smaller magnetic moment, leading to a decrease in M_S. In a word, V_O was produced after neutron irradiation of TiO_2.

The CASTEP module was used to calculate the density of states (DOS) of TiO_2, which is based on a plane wave pseudopotential method and DFT. The electron exchange correlation function is treated using a generalized gradient approximation (GGA) exchange-correlation functional in the form of Perdew–Bruke–Ernzerhof (PBE). GGA+U methods[36,37] were considered to give a proper description of the strong correlation effects. The Hubbard U was employed as $U_{Ti,d} = 6.47$ eV, $U_{O,p} = 4.3$ eV. The Monkhorst–Pack scheme k-point mesh was $2 \times 2 \times 3$ for the $2 \times 2 \times 2$ supercell. The calculation ensured an energy convergence of 1×10^{-6} eV per atom and the cut-off energy was 340 eV.

According to Fig. 6, we can find that the DOS of supercells with V_O, V_{Ti}, and F^+ defects are asymmetric, indicating that supercells with these defects have a magnetic moment. As displayed in Fig. 6(a), pure TiO_2 has symmetric DOS and spin-zero ground states; it does not show magnetism. V_O defects could induce a magnetic moment in TiO_2, as shown in Fig. 6(b). We also calculated F^+, V_{Ti}, $V_{\overline{Ti}}$, Ti^{3+}, O_i, Ti_i, V_O–Ti^{3+}, as shown in Fig. 6(c)–(i). The supercells with F^+ and Ti^{3+} are found to have lower magnetic moments of 1.28 μ_B and 1.70 μ_B, respectively, while the supercell with O_i could not induce a magnetic moment. When there is V_{Ti} or Ti_i, its DOS is spin-polarized and the system has a magnetic moment of ~4 μ_B. The supercell with V_O–Ti^{3+} induces a magnetic moment about the same as that of V_O.

The magnetic moment of the V_O system is 2.39 μ_B. The partial densities of states (PDOS) of Ti with V_O are shown in

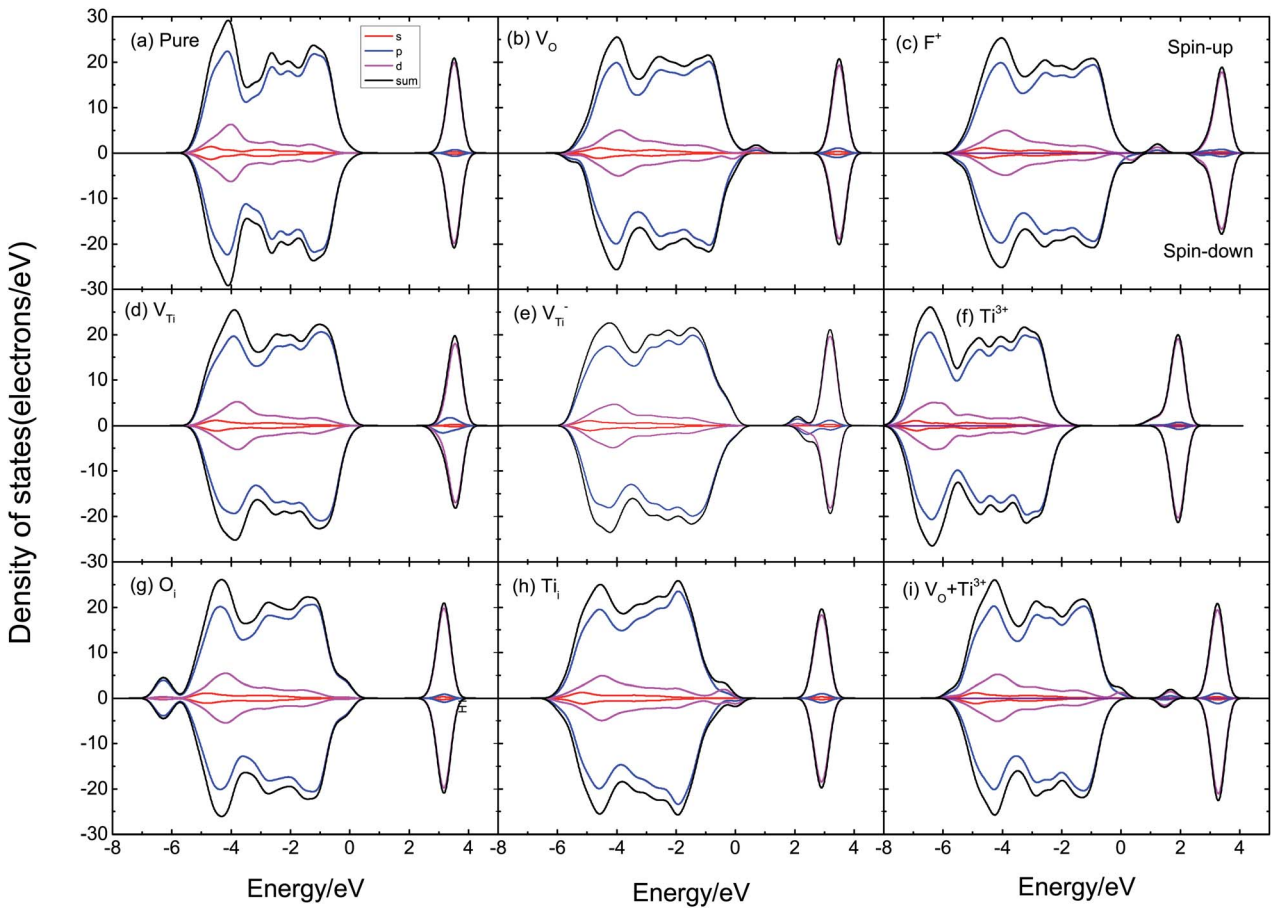

Fig. 6 Spin-polarized total and partial DOS of (a) pure TiO_2, (b) the TiO_2 supercell with one V_O, (c) the TiO_2 supercell with F^+, (d) the TiO_2 supercell with V_{Ti}, (e) the TiO_2 supercell with $V_{\overline{Ti}}$, (f) the TiO_2 supercell with Ti^{3+}, (g) the TiO_2 supercell with O_i, (h) the TiO_2 supercell with Ti_i, (i) the TiO_2 supercell with V_O–Ti^{3+}.

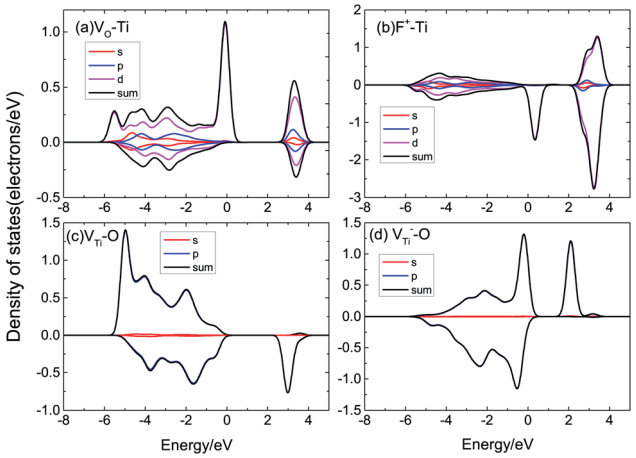

Fig. 7 The PDOS of (a) Ti of V_O, (b) Ti of F^+, (c) O of V_{Ti}, (d) O of V_{Ti}^-.

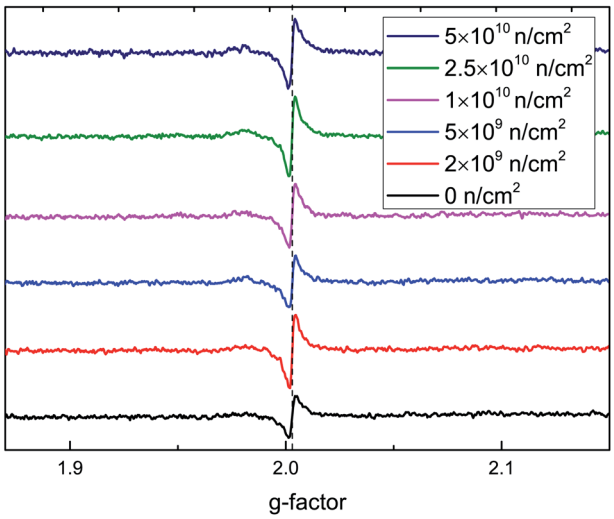

Fig. 8 ESR spectra of TiO_2 before and after neutron irradiation.

Fig. 7(a); the magnetic moment arises from the 3d orbital electrons of the Ti atoms around V_O. When there is V_O, the Ti atoms around V_O are repelled by the V_O, then the electron population of the Ti 3d orbital varies, causing spin-polarization in the system. It can be seen that F^+ induces a 1.28 μ_B magnetic moment. F^+ provides a lower magnetic moment than V_O, as shown in Fig. 7(b); its magnetic moment is also due to the asymmetric PDOS of the Ti 3d orbital. V_{Ti} can induce a 4.53 μ_B magnetic moment due to the O 2p orbital hybridization, as shown in Fig. 7(c). Fig. 7(d) shows the PDOS of O 2p of V_{Ti}^-. For Ti vacancies with various valence states, the titanium vacancy with negatively monovalent charge (V_{Ti}^-) is more stable under different conditions.[38] According to our calculations, V_{Ti}^- induces ~4 μ_B magnetic moment, which is almost consistent with the magnetic moment introduced by the neutral V_{Ti}.

Combining the above experimental and theoretical calculation results, we infer that the magnetism in TiO_2 after D–D neutron irradiation is caused by V_O, V_{Ti} and F^+. Besides, we also calculated the defect formation energies of these kinds of point and compound defects, as shown in Table 2. We used the following formula to calculate defect formation energy (E_f):[39–41]

$$E_f = E_{(D)} - E_{(TiO_2)} + n_1\mu_{(O)} + n_2\mu_{(Ti)} + qE_F \quad (1)$$

$$E_{(TiO_2)} = \mu_{(Ti)} + 2\mu_{(O)} \quad (2)$$

$E_{(D)}$ is the total energy of the supercell with defects (V_O, or V_{Ti}, …), $E_{(TiO_2)}$ is the total energy of pure rutile TiO_2, n_1 and n_2 are the number of removed O (or Ti) atoms, and μ is the chemical potential energy. In the O-rich case, $\mu_{(O)}$ is half of $\mu(O_2)$, $\mu_{(O)} = -430$ eV; $\mu_{(Ti)}$ can be calculated from formula (2), $\mu_{(Ti)} = -1612.04$ eV. In the O-poor case, $\mu_{(Ti)}$ is equal to the metal Ti, and $\mu_{(Ti)}^{metal} = -1602.85$ eV; $\mu_{(O)}$ can be calculated from formula (2), $\mu_{(O)} = -434.58$ eV. q is the charge of the defects, and the Fermi level E_F is the energy of the electron reservoir, referenced to the valence-band maximum (VBM).

The results were different in the O-rich and O-poor cases. V_O is more easily formed than V_{Ti} in terms of the energy of dislocation threshold and defect formation. Therefore, it is easier to form V_O, V_{Ti}, F^+, Ti^{3+} and V_O–Ti^{3+} than Ti_i defects in the atmosphere, and the most likely origin of magnetism in TiO_2 is V_O, V_{Ti}, F^+ and Ti^{3+}. For unirradiated TiO_2, native V_O defects induced RTFM. After D–D neutron irradiation, the defect concentration increases with the irradiation fluence, and the defect type also changes. More and more V_O and V_{Ti} provide conditions for the formation of other defects; Ti^{3+}, F^+ and other compound defects (V_O + Ti^{3+} and so on) are produced, and the density of these defects becomes higher and higher with the increase of neutron irradiation fluence. We also found that V_O can induce a 2.39 μ_B magnetic moment. Ti^{3+} and F^+ defects

Table 2 Formation energy of TiO_2 with neutral intrinsic defects

E_f/eV	V_O	V_{Ti}	O_i	Ti_i
O-rich	7.00	0.57	0.58	11.89
O-poor	2.41	8.62	5.17	2.71

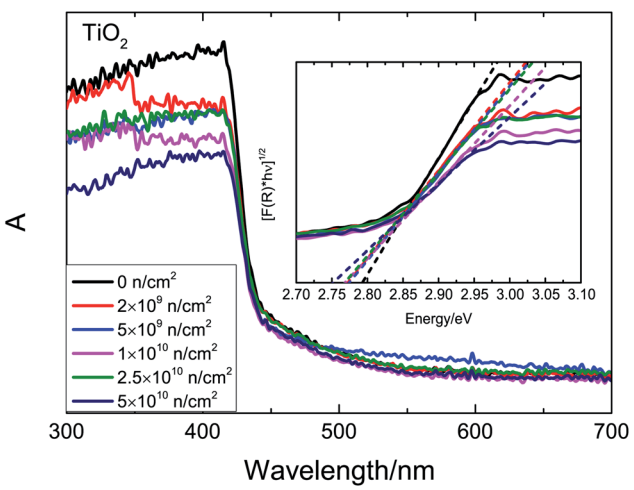

Fig. 9 UV-Vis spectra of TiO_2 before and after neutron irradiation.

introduce smaller magnetic moments that cause the RTFM of the 5×10^9 n cm^{-2} and 1×10^{10} n cm^{-2} samples to decrease. Bao *et al.*[42] proposed that the RTFM may be due to the formation of V_{Ti} from the substitution of Ga for Ti, and V_{Ti} was verified by positron annihilation spectroscopy. Qin *et al.*[43] reported that the RTFM is attributed to V_{Ti} and N_O defects in the rutile structure. Then, more V_{Ti} and V_O play a key role in increasing the RTFM of the 2.5×10^{10} n cm^{-2} and 5×10^{10} n cm^{-2} samples.

To further verify that the RTFM is caused by V_O defects, ESR spectra at 2 K are shown in Fig. 8. A peak was found around a g-factor of 2.003, which was assigned to an oxygen vacancy binding a single electron[44] in rutile TiO_2. The signal intensity first increases and then decreases, then increases with the increase in irradiation fluence, which is in accordance with the M–H curves. From the above analysis, the highest concentration of V_O is induced by 2×10^9 n cm^{-2}; it also causes the greatest changes in magnetism.

The UV-Vis absorption spectra after irradiation are shown in Fig. 9. According to first-principles calculations, a strong absorption at 420 nm is inherent. The optical band gap (E_g) is estimated by the K–M function. The E_g decreases gradually with the increase in fluence. Based on our previous analysis and theoretical research,[14,45] V_O, V_{Ti} and V_O–Ti^{3+} defects introduce unpaired states in the band gap, which could narrow the band gap. As the fluence increases, ever larger concentrations of defects and ever thicker defect states imply an ever narrower band gap. With the increase in irradiation fluence, the total defect concentration increases, and the change of defect types causes the M_s to change.

4 Conclusion

In summary, we found that the origin of RTFM of unirradiated TiO_2 is V_O. D–D neutron irradiation was used to engineer the defect concentration and type. After D–D neutron irradiation, the M_s increases with the increasing concentration of V_O and V_{Ti}. As the neutron irradiation fluence increases, more and more V_O combine electrons to form F^+. F^+ induce a smaller magnetic moment, leading to a decrease in M_s. With further increases of the irradiation fluence, V_{Ti} and V_O play an important role in increasing the magnetic moment. Therefore, RTFM is caused by V_O, F^+, and V_{Ti}. The optimal fluence of D–D neutron irradiation remains to be further explored.

Conflicts of interest

There are no conflicts to declare.

Acknowledgements

This work was supported by the National Natural Science Foundation of China (11575074, 11975006, 11905089), the Key Laboratory of Special Function Materials and Structure Design, Ministry of Education, Lanzhou University (lzujbky-2018-kb06), the Fundamental Research Funds for the Central Universities of Ministry of Education of China (lzujbky-2017-it39, lzujbky-2018-it38), the DSTI Foundation of Gansu (2018ZX-07). A portion of this work was performed at the Steady High Magnetic Field Facilities, High Magnetic Field Laboratory, CAS.

Notes and references

1 U. Bach, D. Lupo, P. Comte, J. E. Moser, F. Weissörtel, J. Salbeck, H. Spreitzer and M. Grätzel, *Nature*, 1998, **395**, 583–585.
2 R. Asahi, T. Morikawa, T. Ohwaki, K. Aoki and Y. Taga, *Science*, 2001, **293**, 269–271.
3 H. Yaghoubi, N. Taghavinia and E. K. Alamdari, *Surf. Coat. Technol.*, 2010, **204**, 1562–1568.
4 V. R. Singh, K. Ishigami, V. K. Verma, G. Shibata, Y. Yamazaki, T. Kataoka, A. Fujimori, F. H. Chang, D. J. Huang and H. J. Lin, *Appl. Phys. Lett.*, 2012, **100**, 242404.
5 S. K. S. Patel, S. Kurian and N. S. Gajbhiye, *AIP Adv.*, 2012, **2**, 012107.
6 A. R. Barman, A. Annadi, K. Gopinadhan, W. M. Lu and T. Venkatesan, *AIP Adv.*, 2012, **2**, 1883.
7 T. C. Kaspar, T. C. Droubay, V. Shutthanandan, S. M. Heald and S. A. Chambers, *Phys. Rev. B: Condens. Matter Mater. Phys.*, 2006, **73**, 155327.
8 H. Saadaoui, X. Luo, Z. Salman, X. Y. Cui, N. N. Bao, P. Bao, R. K. Zheng, L. Tseng, Y. H. Du and T. Prokscha, *Phys. Rev. Lett.*, 2016, **117**, 227202.
9 J. Y. Zheng, S. H. Bao, Y. H. Lv and P. Jin, *ACS Appl. Mater. Interfaces*, 2014, **6**, 22243–22249.
10 Z. Zhou, H. Wang, Z. Zou, D. Meng, J. Guo and Z. Yang, *Mater. Res. Bull.*, 2017, **86**, 287–297.
11 M. Parras, A. Varela, R. Cortes-Gil, K. Boulahya, A. Hernando and J. M. Gonzalez-Calbet, *J. Phys. Chem. Lett.*, 2013, **4**, 2171–2176.
12 W. Songbo, P. Lun, S. Jia-Jia, M. Wenbo, Z. Ji-Jun, W. Li and Z. Xiangwen, *J. Am. Chem. Soc.*, 2015, **137**, 2975–2983.
13 M. Venkatesan, C. B. Fitzgerald and J. M. D. Coey, *Nature*, 2004, **430**, 630.
14 Q. L. Lin, G. P. Li, N. N. Xu, H. Liu and C. L. Wang, *Acta Phys. Sin.*, 2017, **66**, 302–315.
15 H. Liu, G. P. Li, N. N. Xu, Q. L. Lin, L. Yang and C. L. Wang, *Acta Phys. Sin.*, 2016, **65**, 185–193.
16 N. N. Xu, G. P. Li, X. D. Pan and L. M. Bao, *Chin. Phys. B*, 2014, **23**, 10610.
17 H. Liu, G. P. Li, Q. L. Lin, D. J. E, X. D. Gao, X. B. Wei, X. D. Pan, S. X. Zhang, J. J. Ding and W. Lan, *J. Supercond. Novel Magn.*, 2019, **32**, 3557–3562.
18 S. P. S. Porto, P. A. Fleury and T. C. Damen, *Phys. Rev.*, 1967, **154**, 522–526.
19 S. Batakrushna, P. K. Giri, I. Kenji and F. Minoru, *Nanoscale*, 2013, **5**, 5476–5488.
20 M. Higuchi, T. Hosokawa and S. Kimura, *J. Cryst. Growth*, 1991, **112**, 354–358.
21 J. Rodrigues, M. Peres, A. J. S. Fernandes, M. P. F. Graca, N. A. Sobolev, F. M. Costa and T. Monteiro, *Appl. Surf. Sci.*, 2012, **258**, 9143–9147.
22 D. Kim, J. Hong, Y. R. Park and K. J. Kim, *J. Phys.: Condens. Matter*, 2009, **21**, 195405.

23 N. N. Xu, G. P. Li, Q. L. Lin, H. Liu and L. M. Bao, *J. Supercond. Novel Magn.*, 2017, **30**, 1–6.
24 N. N. Xu, G. P. Li, Q. L. Lin, H. Liu and L. M. Bao, *Chin. Phys. B*, 2016, **25**, 106101.
25 X. Wang, Y. Song, L. L. Tao, J. F. Feng, Y. Sui, J. Tang, B. Song, Y. Wang, Y. Wang and Y. Zhang, *Appl. Phys. Lett.*, 2014, **105**, 262402.
26 B. Anitha and M. A. Khadar, *J. Nanopart. Res.*, 2016, **18**, 1–14.
27 J. Li, F. Li, Y. Zhuang, L. Jin, L. Wang, X. Wei, Z. Xu and S. Zhang, *J. Appl. Phys.*, 2014, **116**, 074105.
28 F. Wang, H. Li, Q. Wu, J. Fang, Y. Huang, C. Yin, Y. Xu and Z. Luo, *Electrochim. Acta*, 2016, **202**, 1–7.
29 Z. Zhao, X. Zhang, G. Zhang, Z. Liu, D. Qu, X. Miao, P. Feng and Z. C. Sun, *Nano Res.*, 2015, **8**, 1–11.
30 E. C. Buck, *Radiat. Eff. Defects Solids*, 1995, **133**, 141–152.
31 M. A. Henderson, W. S. Epling, C. H. F. Peden and C. L. Perkins, *J. Phys. Chem. B*, 2003, **107**, 534–545.
32 X. Q. Cheng, C. Y. Ma, X. Y. Yi, F. Yuan, Y. Xie, J. M. Hu, B. C. Hu and Q. Y. Zhang, *Thin Solid Films*, 2016, **615**, 13–18.
33 M. Memesa, S. Lenz, S. G. J. Emmerling, S. Nett, J. Perlich, P. Muller-Buschbaum and J. S. Gutmann, *Colloid Polym. Sci.*, 2011, **289**, 943–953.
34 D. Li, H. Haneda, N. K. Labhsetwar, S. Hishita and N. Ohashi, *Chem. Phys. Lett.*, 2005, **401**, 579–584.
35 L. Kernazhitsky, V. Shymanovska, V. Naumov, L. Fedorenko, V. Kshnyakin, N. Shcherban, S. Filonenko and J. Baran, *J. Lumin.*, 2017, **187**, 521–527.
36 B. J. Morgan and G. W. Watson, *J. Phys. Chem. C*, 2010, **114**, 2321.
37 M. Wang, M. Feng and X. Zuo, *Appl. Surf. Sci.*, 2014, **292**, 475–479.
38 Y. Zhang, N. Ma, M. Zhou, E. Cao, S. Li, W. Hao and Z. Yang, *J. Phys. Chem. Solids*, 2018, **121**, 276–284.
39 S. Naphattalung, M. F. Smith, K. Kim, M. H. Du, S. H. Wei, S. B. Zhang and S. Limpijumnong, *Phys. Rev. B: Condens. Matter Mater. Phys.*, 2006, **73**, 125205.
40 A. Janotti, J. B. Varley, P. Rinke, N. Umezawa, G. Kresse and C. G. Van de Walle, *Phys. Rev. B: Condens. Matter Mater. Phys.*, 2010, **81**, 085212.
41 G. Mattioli, P. Alippi, F. Filippone, R. Caminiti and A. Amore Bonapasta, *J. Phys. Chem. C*, 2010, **114**, 21694–21704.
42 N. N. Bao, J. B. Yi, H. M. Fan, X. B. Qin, P. Zhang, B. Y. Wang, J. Ding and S. Li, *Scr. Mater.*, 2012, **66**, 821–824.
43 X. B. Qin, D. X. Li, R. Q. Li, P. Zhang, Y. X. Li and B. Y. Wang, *Chin. Phys. B*, 2014, **23**, 067502.
44 Q. Jin, Y. Shen, S. Zhu, X. Li and M. Hu, *Chin. J. Catal.*, 2016, **37**, 1521–1528.
45 J. Li, S. Meng, L. Qin and H. Lu, *Chin. Phys. B*, 2017, **26**, 370–375.